

RESEARCH PAPER

Copper Bismuth Oxide/rGO Nanocomposite: Sonochemical Synthesis, Characterization, and Photocatalytic Performance in Dibenzothiophene Desulfurization

Mohammad Reza Tahmasbi, Mehdi Mousavi-Kamazani*, Narjes Keramati

Department of Nanotechnology, Faculty of New Sciences and Technologies, Semnan University, Semnan, Iran

ARTICLE INFO

Article History:

Received 26 April 2024

Accepted 09 June 2024

Published 01 July 2024

Keywords:

$\text{Bi}_{7.38}\text{Cu}_{0.62}\text{O}_{11.69}/\text{rGO}$

Desulfurization

Nanocomposite

Photocatalyst

Sonochemistry

ABSTRACT

Desulfurization of petroleum derivatives is a topic of interest to researchers because compounds containing sulfur are harmful in the oil refining process and cause problems such as deactivation of catalysts and corrosion in pipelines and refining equipment. In order to improve the efficiency of desulfurization of dibenzothiophene, copper bismuth oxide/reduced graphene oxide ($\text{Bi}_{7.38}\text{Cu}_{0.62}\text{O}_{11.69}/\text{rGO}$) nanocomposite was synthesized by a simple sonochemical method for the first time. The synthesized nanocomposite was identified by FESEM, FT-IR, XRD, DRS, and EDS analyses. Based on XRD analysis, pure copper bismuth oxide is formed using hydrazine, while using sodium hydroxide does not lead to the desired product. FESEM images showed that the size of $\text{Bi}_{7.38}\text{Cu}_{0.62}\text{O}_{11.69}$ particles decreases in the presence of rGO. The desulfurization results showed that the presence of rGO causes a significant increase in efficiency due to increased light absorption and reduced recombination rate, so that $\text{Bi}_{7.38}\text{Cu}_{0.62}\text{O}_{11.69}/\text{rGO}$ nanocomposite has an efficiency of 87%, while pure $\text{Bi}_{7.38}\text{Cu}_{0.62}\text{O}_{11.69}$ has an efficiency of 68%. Also, it was found that the purity of the copper bismuth oxide has a great effect on the photocatalytic efficiency, so that by calcining the product and removing the impurities, the efficiency increases from 55% to 68%.

How to cite this article

Tahmasbi M.R., Mousavi-Kamazani M, Keramati N. Copper Bismuth Oxide/rGO Nanocomposite: Sonochemical Synthesis, Characterization, and Photocatalytic Performance in Dibenzothiophene Desulfurization. J Nanostruct, 2024; 14(4):729-740.

DOI: 10.22052/JNS.2024.03.004

INTRODUCTION

Sulfur removal reduces corrosion of refinery equipment such as pumps and pipes [1]. As a result of burning, sulfur-containing compounds turn into sulfur oxides and sulfates and cause acid rains and ultimately harm the environment [1, 2]. Also, sulfur-containing compounds cause poisoning of catalysts during the refining process. As a result, many efforts have been made in many countries of the world to limit sulfur compounds in fuel [1-4]. There are various methods for

desulfurization, including biological, adsorption, extraction, oxidation and hydrogen desulfurization [3]. Meanwhile, photocatalytic oxidative desulfurization (PODS) is an advanced approach in oxidative desulfurization due to its low energy consumption, compatibility with the environment, the ability to use sunlight, and low process cost. In this method, a strong catalyst is used under the influence of light to accelerate the oxidation of sulfur compounds [4-8].

A good photocatalyst should have characteristics



This work is licensed under the Creative Commons Attribution 4.0 International License.

To view a copy of this license, visit <http://creativecommons.org/licenses/by/4.0/>.

such as non-toxicity, optical stability, active in the visible region, high optical activity, and also having a high surface area for maximum pollutant adsorption [8-13]. Copper bismuth oxide as a visible light photocatalyst can offer large pore size and high surface area, which is useful for improving the contact of the active sites of the catalyst with the substrate [14-16]. Since the basis of the photocatalytic method is based on preventing the rapid recombination of the electron-hole pair, this photocatalyst prevented than recombination of the produced electron-hole pairs and ultimately leads to effective separation and Long-term load helps [14, 15]. Also, the use of reduced graphene oxide can play a key role in photocatalytic desulfurization processes by reducing the energy gap and increasing the amount of light absorption, as well as reducing the recombination rate [8, 17, 18].

During many studies, it has been proven that contaminating compounds such as bismuth oxide with metal such as copper, in addition to preventing the recombination of electrons and holes, makes it possible to expand the absorption to the visible region and thus increase the resulting efficiency [19]. Zhang et al. synthesized $\text{CuBi}_2\text{O}_4/\text{CdMoO}_4$ nano-composites with different mass ratios to investigate their photocatalytic activity and enhance their properties for water pollution remediation [15]. During this research, a heterogeneous Z-scheme structure was formed by combining CuBi_2O_4 and CdMoO_4 compounds. By reducing the bandgap, this structure expands the light absorption region from ultraviolet to visible light. Optimal performance in photocatalysis was achieved by $\text{CuBi}_2\text{O}_4/\text{CdMoO}_4$ nanocomposite (10%) with a high degradation rate of 95.36%. Sokhan sanj et al. synthesized the $\text{Bi}_2\text{O}_2\text{CO}_3\text{-CuBi}_2\text{O}_4$ nano-composite with a flower-like morphology using the hydrothermal method and employing ultrasonic waves as an assisting factor [14]. The aim was to investigate its photocatalytic effect in the degradation of malachite green under visible light irradiation. During this study, to investigate the impact of combining the two mentioned phases for enhancing the efficiency of the photocatalyst, the $\text{Bi}_2\text{O}_2\text{CO}_3$ phase was coated on the surface of CuBi_2O_4 and samples with different weight ratios of the $\text{CuBi}_2\text{O}_4\text{-Bi}_2\text{O}_2\text{CO}_3$ nano-composite were prepared. Subsequent examinations revealed that the flower-like morphology, due to its ability to absorb more light with a double-sided surface

area, makes the separation of charge carriers easier. Consequently, with a reduction in the recombination rate of electron-hole pairs, it leads to an increase in the photocatalytic efficiency.

In the current study, with the aim of enhancing surface adsorption and increasing light absorption in the visible range, copper bismuth oxide has been utilized as an excellent photocatalyst in sulfur removal processes under visible light irradiation along with reduced graphene oxide. The use of rGO is considered a suitable option due to its significantly higher thermal stability compared to GO, as well as its flexibility between molecules, leading to increased surface adsorption and light absorption [17, 18]. Hydrazine has been employed as a reducing agent to convert graphene oxide (GO) to reduced graphene oxide (rGO). The sonochemical method was chosen for the synthesis of the $\text{Bi}_{7.38}\text{Cu}_{0.62}\text{O}_{11.69}/\text{rGO}$ nanocomposite due to its ease of execution, low temperature, high speed, and the ability to control factors influencing the reaction. Additionally, XRD, FTIR, EDS, DRS, and FESEM analyses were employed to determine the morphology and structure of the nanocomposite. Finally, the performance of this nanocomposite was evaluated for desulfurization of dibenzothiophene as a representative of petroleum liquids. According to our knowledge, the use of this synthetic method for the production of the mentioned nanocomposite is reported for the first time.

MATERIALS AND METHODS

Instruments and materials

All materials used in this research, including copper nitrate trihydrate ($\text{Cu}(\text{NO}_3)_2 \cdot 3\text{H}_2\text{O}$), bismuth(III) nitrate pentahydrate ($\text{Bi}(\text{NO}_3)_3 \cdot 5\text{H}_2\text{O}$), bismuth(III) nitrate ($\text{Bi}_5\text{H}_9\text{N}_4\text{O}_{22}$), potassium permanganate (KMnO_4), sodium hydroxide (NaOH), graphite, $\text{N}_2\text{H}_4 \cdot \text{H}_2\text{O}$ (80%), hydrochloric acid (HCl), sulfuric acid (H_2SO_4), normal hexane (C_6H_{14}), benzothiophene ($\text{C}_8\text{H}_6\text{S}$), and hydrogen peroxide (H_2O_2) were purchased from Merck and Sigma-Aldrich companies and were used without further purification. Ultrasound was performed using an ultrasonic 12 mm diameter probe, operating at 20 kHz with an output power of 400 Wcm^{-2} . MIRA3 FEGSEM was utilized for recording FESEM (field emission scanning electron microscope) images. XRD (X-ray diffraction) patterns were examined with a Philips-X'PertPro instrument employing Ni-filtered $\text{Cu K}\alpha$ radiation.

EDS (energy dispersive spectroscopy) was conducted utilizing a Philips XL30 X-ray scattering apparatus. FT-IR (Fourier transform infrared) analysis was executed using a Magna-IR device, specifically a Nicolet 550 spectrometer, with a resolution of 0.125 cm on KBr tablets spanning the range of 400 to 4000 cm^{-1} . DRS (diffuse reflectance spectrometry) analysis was conducted using the Shimadzu model UV3600Iplus. A sulfur analyzer in oil model Horiba-SLFA-20 was employed for measure sulfur levels.

Synthesis of rGO suspension

First, GO (graphene oxide) was produced by Hummer’s advanced method [20]. Then, 0.1 g of graphene oxide along with 50 ml of distilled water was poured into a beaker and placed on a stirrer to facilitate mixing. Subsequently, 5 ml of hydrazine, as a reducing agent, was added drop by drop to the solution. Next, the beaker content was transferred to an autoclave and heated at 180 °C for 16 hours. After cooling the autoclave to room temperature, the resulting suspension was removed from the autoclave.

Synthesis of $\text{Bi}_{7.38}\text{Cu}_{0.62}\text{O}_{11.69}/\text{rGO}$ nanocomposite

First, 5 ml of hydrazine was mixed with 40 ml of distilled water and exposed to ultrasonic waves with a power of 100 watts for 3 minutes (solution A). Then, in a separate beaker, 2.922 g of bismuth salt and 0.241 g of copper nitrate salt were dissolved in 40 ml of distilled water and solution B was prepared. Solution B was added to solution A and the irradiation with ultrasonic waves continued for another 10 minutes. Afterwards, the rGO suspension synthesized in the previous step was added to the above mixture. The resulting mixture was exposed to ultrasonic waves with a power of 100 watts for 10 minutes. Finally, the final sediment was collected and dried in an oven at 70 °C after washing with water and ethanol (sample S2). Fig. 1 shows the synthesis steps of sample S2 ($\text{Bi}_{7.38}\text{Cu}_{0.62}\text{O}_{11.69}/\text{rGO}$ nanocomposite). For the synthesis of $\text{Bi}_{7.38}\text{Cu}_{0.62}\text{O}_{11.69}$ (sample S1), the above steps were repeated and only rGO was not used. In order to reveal the role of hydrazine on the purity and structure of the product, an experiment was performed using sodium hydroxide and nitric

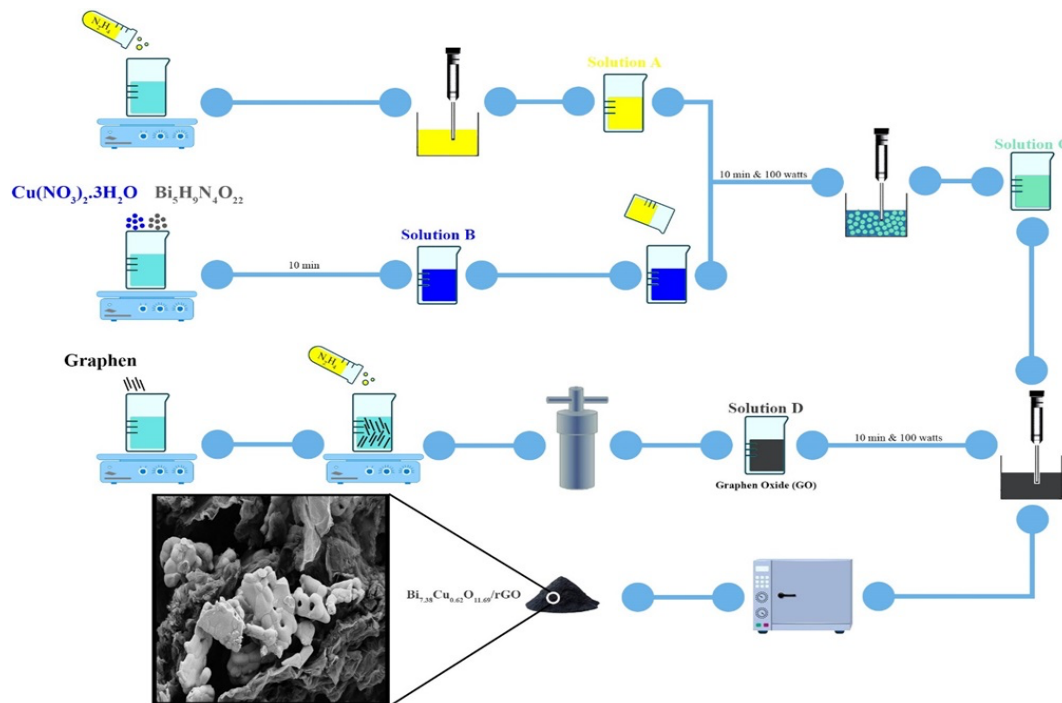


Fig. 1. Synthesis steps of $\text{Bi}_{7.38}\text{Cu}_{0.62}\text{O}_{11.69}/\text{rGO}$ nanocomposite.

Table 1. Reaction conditions for the preparation of $\text{Bi}_{7.38}\text{Cu}_{0.62}\text{O}_{11.69}/\text{rGO}$ nanocomposite under 100 W ultrasonic waves.

| Sample NO | Bi Salt | OH^- Source | | HNO_3 (ml) | Temp ($^\circ\text{C}$) | rGO (g) | Product |
|-----------|--|----------------------|-------------------|---------------------|---------------------------|--|---|
| | | Hydrazine (ml) | NaOH (0.6 M) (ml) | | | | |
| S1 | $\text{Bi}_5\text{H}_9\text{N}_4\text{O}_{22}$ | 5 | ---- | ---- | ---- | ---- | Amorphous |
| S1-C | | | 500 | | | $\text{Bi}_{7.38}\text{Cu}_{0.62}\text{O}_{11.69}/\text{Bi}_2\text{CuO}_4$ | |
| S2 | $\text{Bi}_5\text{H}_9\text{N}_4\text{O}_{22}$ | 5 | ---- | ---- | ---- | 0.1 | $\text{Bi}_{7.38}\text{Cu}_{0.62}\text{O}_{11.69}/\text{rGO}$ |
| S3 | $\text{Bi}_5\text{H}_9\text{N}_4\text{O}_{22}$ | ---- | 30 | 3 | ---- | - | $\text{Bi}_2\text{O}_3/\text{Bi}(\text{Bi}_6\text{O}_6(\text{OH})_2)(\text{OH})$ |
| S4 | $\text{Bi}_5\text{H}_9\text{N}_4\text{O}_{22}$ | ---- | 30 | 3 | ---- | 0.1 | $\text{Bi}_2\text{O}_3/\text{Bi}(\text{Bi}_6\text{O}_6(\text{OH})_2)(\text{OH})/\text{rGO}$ |
| S5 | $\text{Bi}(\text{NO}_3)_3 \cdot 5\text{H}_2\text{O}$ | 5 | ---- | ---- | ---- | ---- | $\text{Bi}_6\text{H}_9\text{N}_5\text{O}_{26}/\text{Bi}_2\text{O}_3$ |

acid (the usual method of copper bismuth oxide synthesis) instead of hydrazine (Sample S3). Due to the difficult solubility of bismuth salts, one of the factors affecting the purity of the product is the type of bismuth source. Therefore, an experiment was conducted using $\text{Bi}(\text{NO}_3)_3 \cdot 5\text{H}_2\text{O}$ instead of $\text{Bi}_5\text{H}_9\text{N}_4\text{O}_{22}$ (Sample S5). The synthesis conditions of the products are presented in Table 1.

Photocatalytic desulfurization of dibenzothiophene

At first, 500 ml of a solution of 800 ppm with respect to sulfur was prepared from dibenzothiophene. Afterwards 120 ml of standard solution and 0.12 g of the photocatalyst powder were poured into the beaker, and the beaker was placed inside the reactor. In order to balance between adsorption and desorption, the obtained mixture was stirred for 30 minutes in the dark under aeration and then exposed to a 400 W Osram visible lamp for 40 minutes. To measure sulfur, 15 ml of samples were collected at certain time intervals and then the photocatalyst was separated using a centrifuge. The remaining solution was washed with acetonitrile and its sulfur content was determined using a sulfur-in-oil measuring instrument.

RESULTS AND DISCUSSION

XRD studies

In order to find out the phase composition of the product and determine its crystal structure, X-ray diffraction analysis (XRD) was used. Fig. 2 shows the X-ray diffraction pattern for samples S1, S1-c, S2, S3, and S5. As seen in Fig. 2a, the pattern of the product synthesized using hydrazine (sample S1) is amorphous, which can be affected by the use of ultrasound waves. By calcining sample S1 at 500 $^\circ\text{C}$ (sample S1-c), several peaks appeared in the pattern, which correspond to copper bismuth oxide with a tetragonal phase

of $\text{Bi}_{7.38}\text{Cu}_{0.62}\text{O}_{11.69}$ (JCPDS = 1765-049-00 and lattice parameters $a = b = 7.73 \text{ \AA}$, and $c = 5.63 \text{ \AA}$) and a tetragonal phase of Bi_2CuO_4 (JCPDS = 01-080-0993 and lattice parameters $a = b = 8.4989 \text{ \AA}$, and $c = 5.7973 \text{ \AA}$) (Fig. 2b). Fig. 2c corresponds to sample S2 synthesized using reduced graphene oxide (rGO). The peaks in Fig. 2c are in good agreement with $\text{Bi}_{7.38}\text{Cu}_{0.62}\text{O}_{11.69}$. The absence of the peak at the angle of 10.64° also shows that graphene oxide (GO) has been converted to reduced graphene oxide (rGO) [21]. Normally, nitric acid and sodium hydroxide are used for the synthesis of copper bismuth oxide [16]. The pattern of the product synthesized using nitric acid and sodium hydroxide (sample S3) is presented in Fig. 2d, and it is clear that the peaks mainly correspond to Bi_2O_3 with tetragonal phase (JCPDS=00-22-0515 and lattice parameters $a=b=10.94 \text{ \AA}$, and $c=11.28 \text{ \AA}$) and copper bismuth oxide was not synthesized. As an OH^- donor, hydrazine can supply OH^- in a controlled manner compared to sodium hydroxide, thus paving the way for the production of copper bismuth oxide. As a result, copper bismuth oxide can be synthesized through sonochemical method using hydrazine. It is worth mentioning that in this research, in order to investigate the effect of changing the input source of bismuth in the reaction environment, which was the same as dry bismuth salt, the use of aqueous bismuth was considered in the synthesis of sample 5. It was determined that due to the low solubility of aqueous bismuth in the synthesis process, it introduces impurities. The average crystallite size of copper bismuth oxide in sample S1, obtained using the Scherrer's equation [22], was approximately 36 nm.

FTIR spectrum studies

FTIR spectroscopy was used to investigate the chemical bonds and organic groups, and the

results are displayed in Fig. 3. In the spectrum of all five samples (samples S1, S1-C, S2, S3, and S4), the peaks at $480\text{ cm}^{-1} \sim 800\text{ cm}^{-1}$ correspond to the stretching vibrations of Bi-O and Cu-O bonds [19, 22-24]. Also, the peaks around 1629 cm^{-1} and 3434 cm^{-1} in all five samples belong to the stretching and bending vibrations of the O-H bond, which

indicates the absorption of water molecules [25]. In the spectrum of sample S1 (Fig. 3a), a number of additional peaks can be seen, which are related to organic compounds caused by the presence of hydrazine on the surface of the sample. After calcination of sample S1, the mentioned peaks have been removed (Fig. 3b). Fig. 3c is related to

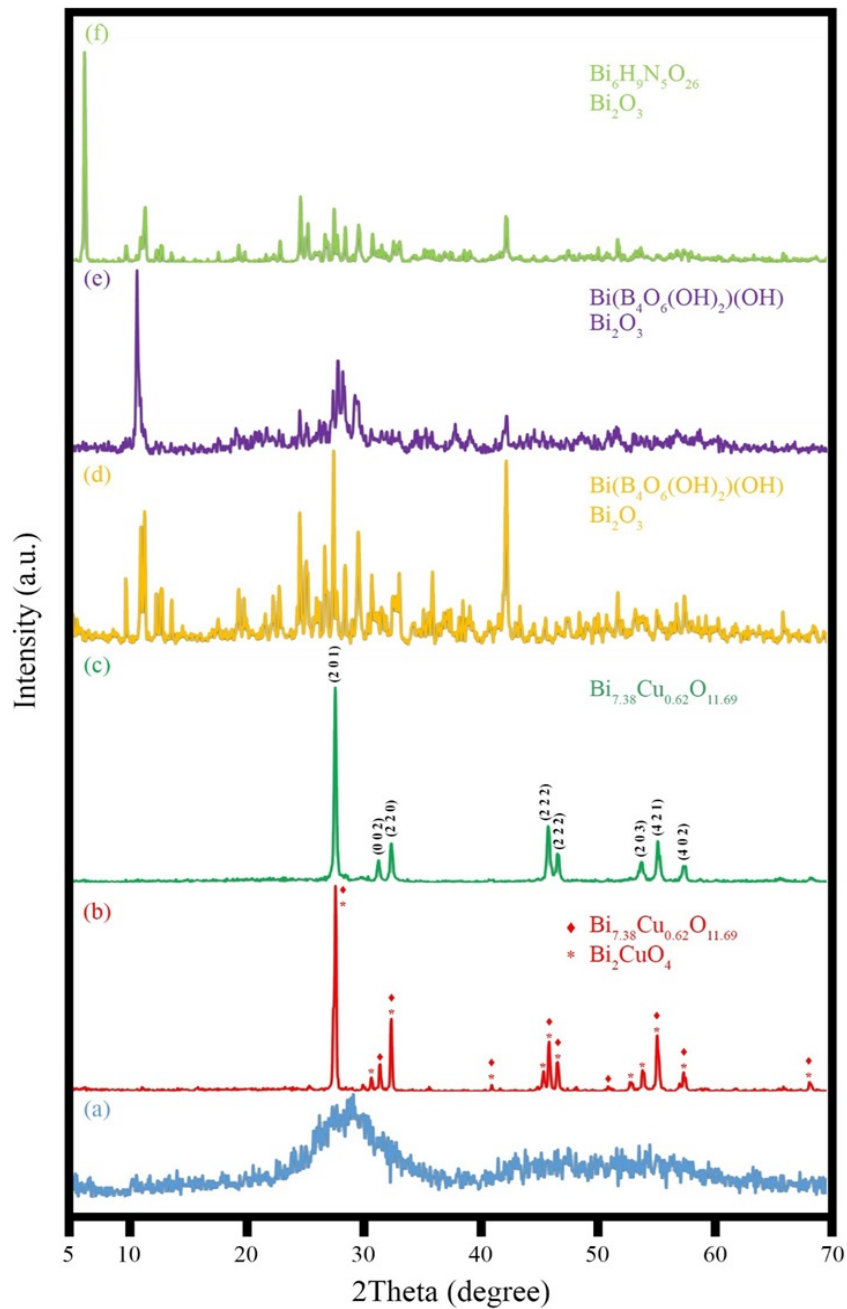


Fig. 2. XRD patterns of the as-synthesized products (a) sample S1, (b) sample S1 after calcination, (c) sample S2, (d) sample S3, (e) sample S4, and (f) sample S5.

the synthesized $\text{Bi}_{7.38}\text{Cu}_{0.62}\text{O}_{11.69}/\text{rGO}$ (sample S2) composite. The absence of peaks related to functional groups containing oxygen such as C-OH, C-O-C and C=O in Fig. 3c shows that graphene oxide has been reduced to graphene [26, 27]. In order to further investigate the FTIR spectra of samples S3 and S4, which were synthesized in the absence

and presence of rGO, respectively, are presented in Figs. 3d and e. The difference in the peaks of these two samples with the peaks of samples S1 and S2, especially in the region of $400\text{--}800\text{ cm}^{-1}$, due to the different synthesized compounds, is fully expected and in accordance with the XRD results. Comparing the IR spectrum of sample

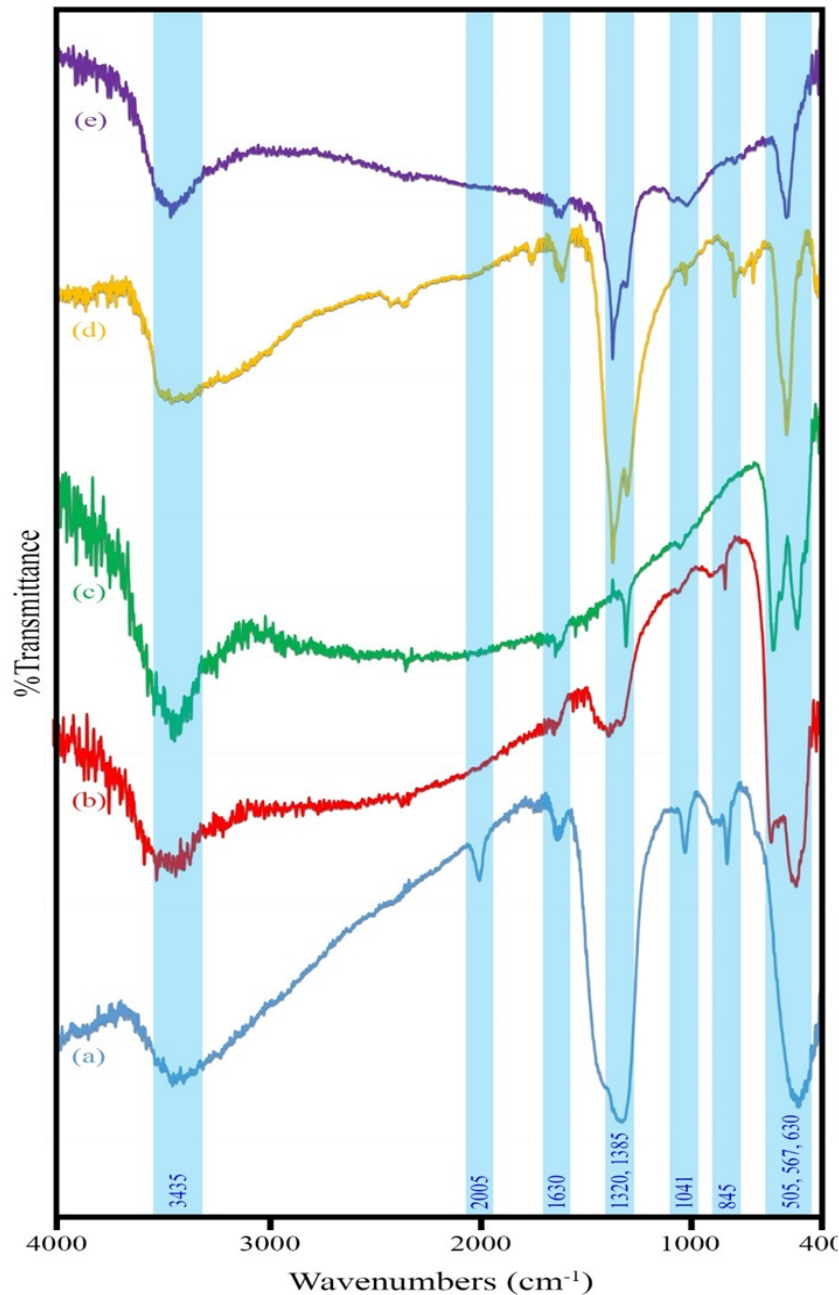


Fig. 3. FT-IR spectra of the as-synthesized products (a) sample S1, (b) sample S1 after calcination ($\text{Bi}_{7.38}\text{Cu}_{0.62}\text{O}_{11.69}$), (c) sample S2 ($\text{Bi}_{7.38}\text{Cu}_{0.62}\text{O}_{11.69}/\text{rGO}$), (d) sample S3, and (e) sample S4.

S3 with sample S4 also shows that there is no additional peak related to carbon-oxygen bonds in sample S4, and in other words, it can be said with certainty that GO has been converted to rGO [28].

EDS studies

Figs. 4a-d show the EDS spectra of samples S1 after calcination ($\text{Bi}_{7.38}\text{Cu}_{0.62}\text{O}_{11.69}$), S2 ($\text{Bi}_{7.38}\text{Cu}_{0.62}\text{O}_{11.69}/\text{rGO}$), S3, and S5, respectively. In Fig. 4a, which corresponds to sample S1 after calcination, only copper, bismuth, and oxygen elements can be seen and no other elements are seen. In the spectrum of $\text{Bi}_{7.38}\text{Cu}_{0.62}\text{O}_{11.69}/\text{rGO}$ nanocomposite (sample S2), in addition to copper, bismuth, and oxygen elements that represent $\text{Bi}_{7.38}\text{Cu}_{0.62}\text{O}_{11.69}$, carbon element is also observed, which indicates the composition of rGO (Fig. 4b). As observed in Fig. 4c, due to the use of nitric acid in the synthesis path of sample S3, the percentage of bismuth is high, and the amount of copper is negligible. This is consistent with the XRD results, which indicate the formation of bismuth oxide as a by-product. In the EDS spectrum of sample 5 (Fig. 4d), which was synthesized using aqueous bismuth salt, only

bismuth and oxygen elements can be seen, which confirms the XRD results, that is, the formation of bismuth oxide instead of copper bismuth oxide.

EDS mapping studies

In order to investigate the dispersion and distribution of the elements in the product, an element dispersion analysis was prepared from sample S2 ($\text{Bi}_{7.38}\text{Cu}_{0.62}\text{O}_{11.69}/\text{rGO}$) (Fig. 5). As can be seen in Fig. 5, only the expected elements such as copper, bismuth, oxygen and carbon are present in the sample. Although copper bismuth oxide is placed on graphene oxide in many places, but because the synthesis method of this sample was two-step, i.e. copper bismuth oxide was first synthesized and then spread on the reduced graphene oxide, complete uniformity is not seen.

FESEM studies

FESEM images of samples S1 and S2 synthesized using hydrazine in the absence and presence of rGO, respectively, are presented in Fig. 6. According to Fig. 6a, in the absence of rGO, rod-like copper bismuth oxide microstructures are formed. In the presence of rGO (sample S2), microstructures with

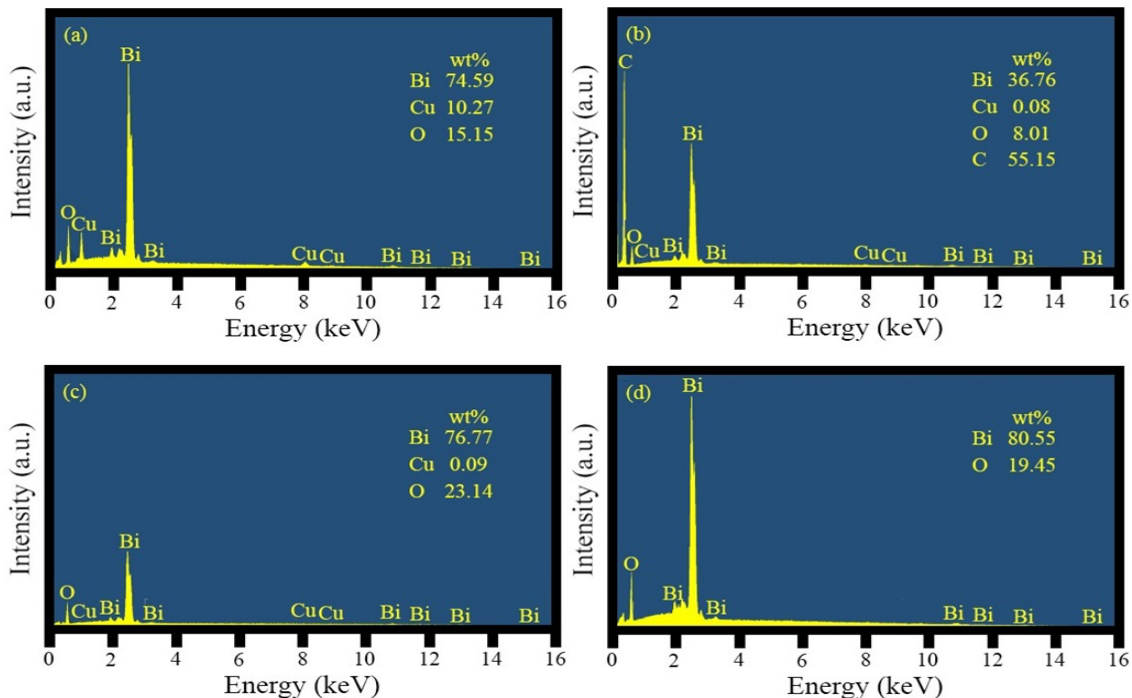


Fig. 4. EDS spectra of the as-synthesized products (a) sample S1 after calcination ($\text{Bi}_{7.38}\text{Cu}_{0.62}\text{O}_{11.69}$), (b) sample S2 ($\text{Bi}_{7.38}\text{Cu}_{0.62}\text{O}_{11.69}/\text{rGO}$), (c) sample S3, and (d) sample S5.



smaller size are formed on graphene sheets (Fig. 6b). Graphene controls the growth of particles by creating a suitable substrate for copper bismuth oxide nucleation. Fig. 7, which is related to the SEM images of samples S3 and S4, which were synthesized using sodium hydroxide in the absence and presence of graphene, respectively, shows the effect of graphene on the structure better. According to Fig. 7a, in the absence of rGO, rod-shaped copper bismuth microstructures have been synthesized, while in the presence of rGO, these structures are broken and nanometer structures are formed on graphene at many places (Fig. 7b).

DRS analysis

The absorption spectra of samples S1, S1 after calcination ($\text{Bi}_{7.38}\text{Cu}_{0.62}\text{O}_{11.69}$), S2 ($\text{Bi}_{7.38}\text{Cu}_{0.62}\text{O}_{11.69}/\text{rGO}$), and S3 ($\text{Bi}_2\text{O}_3/\text{Bi}(\text{B}_4\text{O}_6(\text{OH})_2)(\text{OH})$) are shown in Fig. 8. As can be seen, all samples show high absorption in the ultraviolet range. Comparing Figs. 8a and 8b shows that by calcining sample S1, due to the formation of copper bismuth oxide with higher purity, the amount of light absorption increases in the region of 700-400 nm. As expected, due to the presence of rGO, sample S2 has a wide absorption in both ultraviolet and especially visible regions (Fig. 8c). Sample S3, which was synthesized using sodium

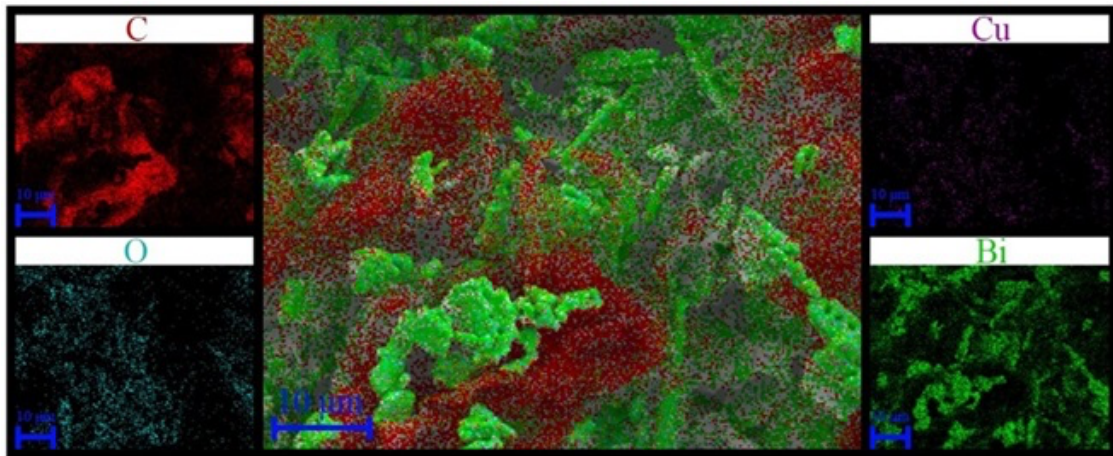


Fig. 5. EDS mapping of the as-synthesized $\text{Bi}_{7.38}\text{Cu}_{0.62}\text{O}_{11.69}/\text{rGO}$ nanocomposite (sample S2).

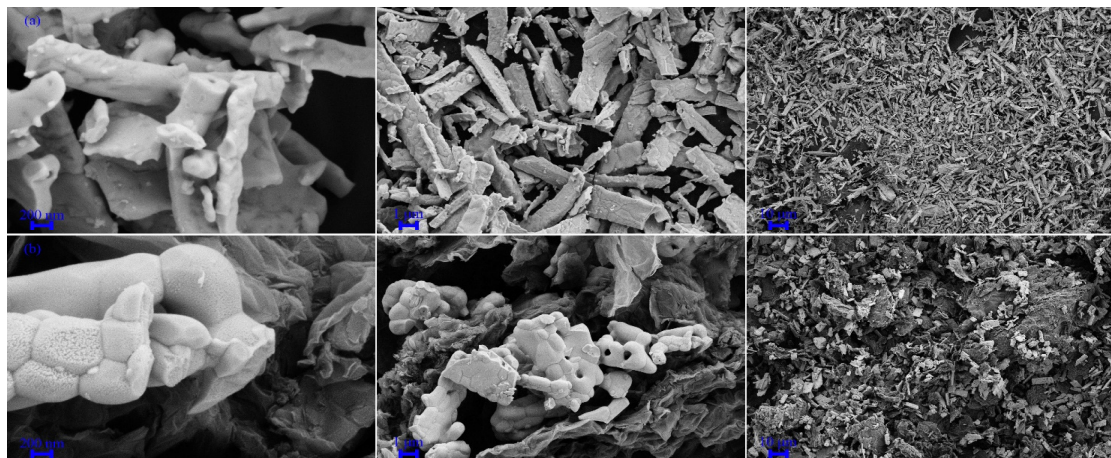


Fig. 6. FESEM images of the as-synthesized products (a-c) sample S1 after calcination ($\text{Bi}_{7.38}\text{Cu}_{0.62}\text{O}_{11.69}$) and (d-f) sample S2 ($\text{Bi}_{7.38}\text{Cu}_{0.62}\text{O}_{11.69}/\text{rGO}$).

hydroxide instead of hydrazine, has very weak absorption in the visible region (Fig. 8d). According to the XRD results, the reason can be the lack of production of copper bismuth oxide.

Photocatalytic desulfurization of dibenzothiophene

Fig. 9 presents the results of photocatalytic

oxidative desulfurization of dibenzothiophene by the synthesized products. As shown in Fig. 9, the highest efficiency, which is about 87%, was obtained for sample S2 ($\text{Bi}_{7.38}\text{Cu}_{0.62}\text{O}_{11.69}/\text{rGO}$). According to the DRS spectra (Fig. 8), sample S2, which contains copper bismuth oxide (without impurities) and rGO, has the highest amount

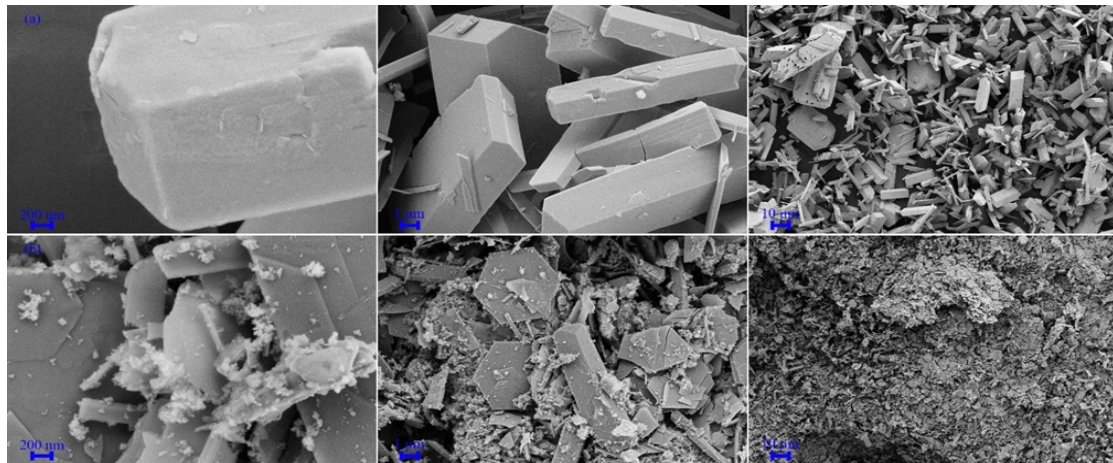


Fig. 7. FESEM images of the as-synthesized products (a-c) sample S3 and (d-f) sample S4.

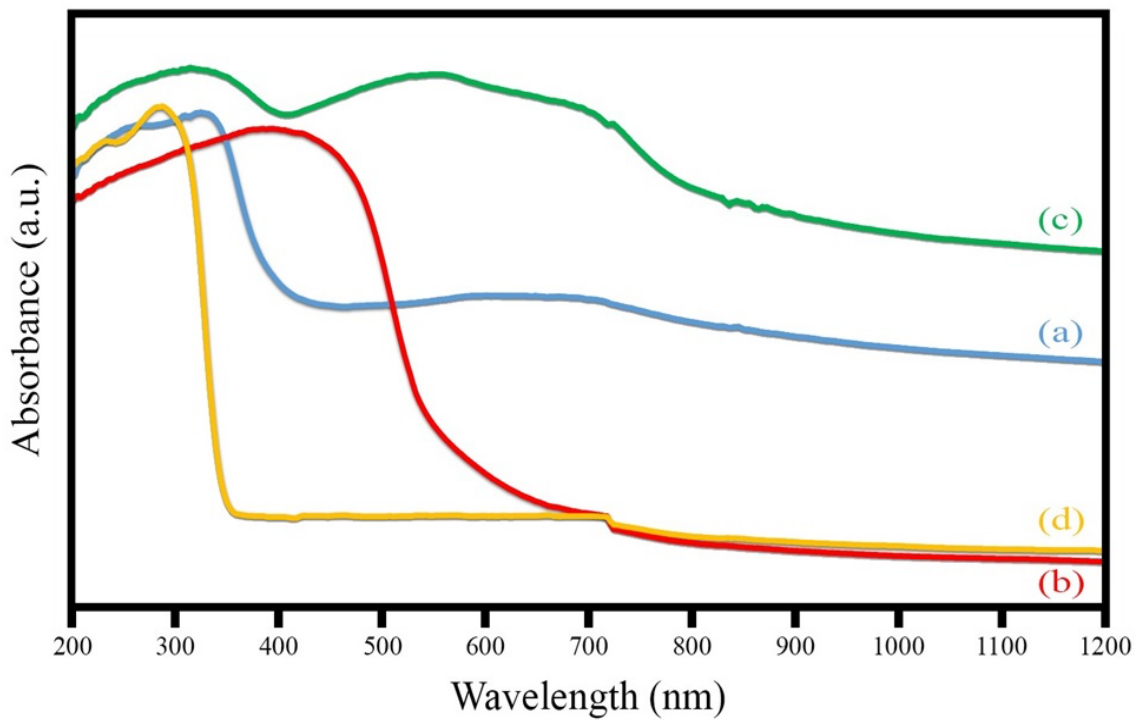


Fig. 8. Absorbance spectra of the as-synthesized products (a) sample S1, (b) sample S1 after calcination ($\text{Bi}_{7.38}\text{Cu}_{0.62}\text{O}_{11.69}$), (c) sample S2 ($\text{Bi}_{7.38}\text{Cu}_{0.62}\text{O}_{11.69}/\text{rGO}$), and (d) sample S3 ($\text{Bi}_2\text{O}_3/\text{Bi}(\text{B}_4\text{O}_6(\text{OH})_2)(\text{OH})$).

of light absorption. Also, compared to sample S4, which was synthesized using soda, it has no impurities. Comparing the efficiency of sample S1 before (55%) and after calcination (68%) shows that the higher the purity of copper bismuth oxide, the higher the efficiency. In addition to high

light absorption, rGO reduces the electron-hole recombination and increases the photocatalytic efficiency [17, 27, 28]. This issue is well confirmed by comparing the efficiency of samples S2 (87%) and S4 (62%) that have rGO with the efficiency of samples S1 (68%) and S3 (58%) that do not have

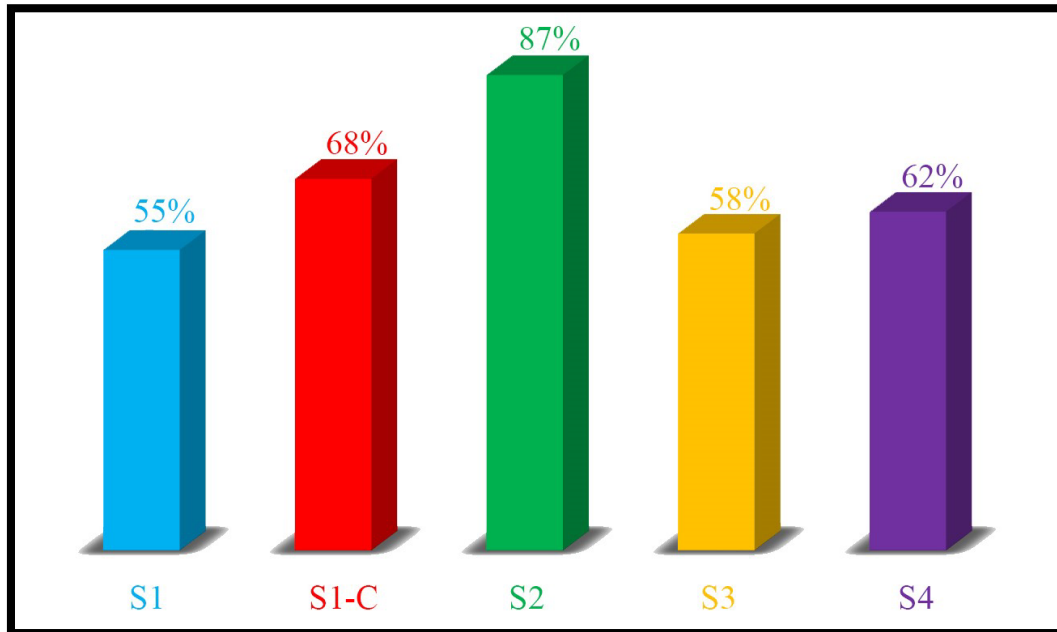


Fig. 9. Percentage of photocatalytic oxidative desulfurization of dibenzothiophene by synthesized products.

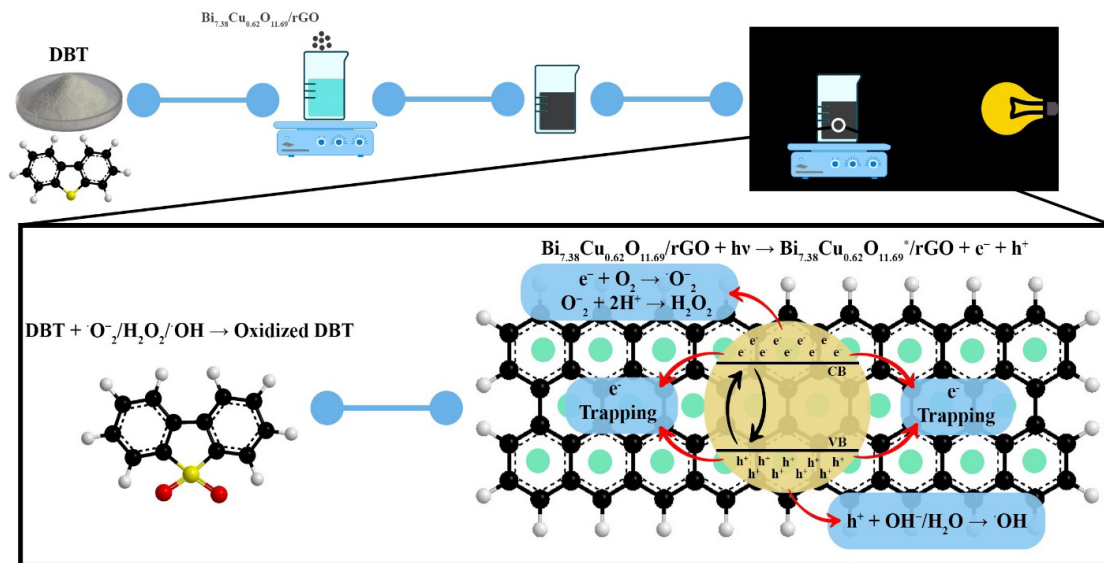


Fig. 10. Proposed mechanism for photocatalytic oxidative desulfurization of dibenzothiophene by $\text{Bi}_{7.38}\text{Cu}_{0.62}\text{O}_{11.69}/\text{rGO}$ nanocomposite.

rGO. The proposed mechanism for photocatalytic oxidative desulfurization of dibenzothiophene by $\text{Bi}_{7.38}\text{Cu}_{0.62}\text{O}_{11.69}/\text{rGO}$ nanocomposite is presented in Fig. 10.

CONCLUSION

In this research, copper bismuth oxide/reduced graphene oxide nanocomposite was synthesized by sonochemical method and its photocatalytic activity was studied in removing sulfur from dibenzothiophene. In order to convert graphene oxide to reduced graphene oxide, hydrazine was used as a reducing agent. The products were characterized using XRD, EDS, FESEM, FT-IR, and DRS analyzes. The desulfurization efficiency of $\text{Bi}_{7.38}\text{Cu}_{0.62}\text{O}_{11.69}/\text{rGO}$ nanocomposite was determined as 87%. From the efficiency comparison between the nanocomposites containing rGO (87%) and the synthesized nanostructures without rGO (68%), it was found that there is a significant increase in the desulfurization efficiency. This improvement is attributed to the heightened light absorption, increased active sites, and the concurrent reduction in the electron-hole recombination rate facilitated by rGO. This study provided new insight into the fabrication and practical application of high performance $\text{Bi}_{7.38}\text{Cu}_{0.62}\text{O}_{11.69}/\text{rGO}$ photocatalyst for desulfurization of petroleum derivatives.

ACKNOWLEDGMENT

The authors would like to thank Semnan University Research Council for the financial support of this work.

CONFLICT OF INTEREST

The authors declare that there is no conflict of interests regarding the publication of this manuscript.

REFERENCES

- Zaidi Z, Gupta Y, Gayatri SL, Singh A. A comprehensive discussion on fuel combustion and desulfurization technologies. *Inorg Chem Commun*. 2023;154:110964.
- Izadi R, Assarian D, Altaee A, Mahinroosta M. Investigation of methods for fuel desulfurization wastewater treatment. *Chem Eng Res Des*. 2023;190:198-219.
- Raeisi A, Najafi Chermahini A, Momeni MM. A novel photocatalytic and photoelectrocatalytic system for oxidative desulfurization of model fuel using BiVO_4 @HKUST-1 composite in powder and deposited on fluorine-doped tin oxide. *J Photochem Photobiol A: Chem*. 2022;433:114190.
- Beshtar M, Khorasheh F, Larimi A, Akbar Asgharinezhad A. Photocatalytic oxidative desulfurization of model fuel using iron-molybdenum nanocatalyst based on cerium oxide (FeyMox/CeO_2) under visible light. *Fuel*. 2024;360:130549.
- Hitam CNC, Jalil AA, Abdulrasheed AA. A review on recent progression of photocatalytic desulphurization study over decorated photocatalysts. *Journal of Industrial and Engineering Chemistry*. 2019;74:172-186.
- Zhou X, Wang T, Liu H, Gao X, Wang C, Wang G. Desulfurization through Photocatalytic Oxidation: A Critical Review. *ChemSusChem*. 2020;14(2):492-511.
- Zhen Y, Wang J, Fu F, Fu W, Liang Y. The Novel Z-Scheme Ternary-Component $\text{Ag/AgI}/\alpha\text{-MoO}_3$ Catalyst with Excellent Visible-Light Photocatalytic Oxidative Desulfurization Performance for Model Fuel. *Nanomaterials*. 2019;9(7):1054.
- Deng C, Lv Y, sun m, Yaseen M, li s, wang l. Phosphomolybdic Acid Clusters and Carbon Nitride Co-loading on $\text{Nh}_2\text{-N-Rgo}$ for Photocatalytic Oxidation Desulfurization. *Elsevier BV*; 2023.
- Jamdar M, Monsef R, Ganduh SH, Dawi EA, Jasim LS, Salavati-Niasari M. Unraveling the potential of sonochemically achieved $\text{DyMnO}_3/\text{Dy}_2\text{O}_3$ nanocomposites as highly efficient visible-light-driven photocatalysts in decolorization of organic contamination. *Ecotoxicology and Environmental Safety*. 2024;269:115801.
- Etmnan M, Nabiyouni G, Ghanbari D. Preparation of tin ferrite-tin oxide by hydrothermal, precipitation and auto-combustion: photo-catalyst and magnetic nanocomposites for degradation of toxic azo-dyes. *Journal of Materials Science: Materials in Electronics*. 2017;29(3):1766-1776.
- Beshkar F, Zinatloo-Ajabshir S, Salavati-Niasari M. Preparation and characterization of the CuCr_2O_4 nanostructures via a new simple route. *Journal of Materials Science: Materials in Electronics*. 2015;26(7):5043-5051.
- Jafarnejad A, Salavati-Niasari M, Monsef R, Bashiri H. Flower-shaped magnetically recyclable $\text{ZnS/ZnIn}_2\text{S}_4/\text{Fe}_2\text{O}_3$ nanocomposites towards decolorization of colored pollutants. *International Journal of Hydrogen Energy*. 2023;48(9):3440-3455.
- Zinatloo-Ajabshir S, Morassaei MS, Salavati-Niasari M. Eco-friendly synthesis of $\text{Nd}_2\text{Sn}_2\text{O}_7$ -based nanostructure materials using grape juice as green fuel as photocatalyst for the degradation of erythrosine. *Composites Part B: Engineering*. 2019;167:643-653.
- Sokhansanj A, Haghghi M, Shabani M. Macroporous flowerlike $\text{Bi}_2\text{O}_2\text{CO}_3\text{-CuBi}_2\text{O}_4$ nanoheterojunction photocatalyst for high concentrated malachite green degradation: Influence of nanocomposite composition and sonication approach. *J Mol Liq*. 2023;371:121024.
- Zhang X, Wang S, Lin L, Tan X, Zeng Y. Design of a novel $\text{CuBi}_2\text{O}_4/\text{CdMoO}_4$ heterojunctions with nano-microsphere structure: Synthesis and photocatalytic degradation mechanism. *Colloids Surf Physicochem Eng Aspects*. 2021;614:126008.
- Chen J, Yao L, Chen X, Li N, Yu C, Zhang Y, Lai Y. Hydrothermal synthesis of dendritic CuBi_2O_4 and its photocatalytic performance towards tetracycline degradation under different light conditions. *Mater Sci Semicond Process*. 2022;142:106503.
- Phadi BM, Oyewo OA, Ramaila S, Mavuru L, Onwudiwe DC. Nanocomposite of $\text{CeVO}_4/\text{BiVO}_4$ Loaded on Reduced Graphene Oxide for the Photocatalytic Degradation of

- Methyl Orange. *Journal of Cluster Science*. 2021;33(6):2707-2721.
18. Farahani M, Mousavi-Kamazani M, Salarvand Z. Synthesis and characterization of $\text{Ce}_{0.5}\text{Bi}_{0.5}\text{VO}_4/\text{rGO}$ nanocomposite by sonochemical method for photocatalytic desulfurization of petroleum derivatives. *Sci Rep*. 2023;13(1).
 19. Mousavi-Kamazani M. Cube-like $\text{Cu}/\text{Cu}_2\text{O}/\text{BiVO}_4/\text{Bi}_7\text{VO}_{13}$ composite nanoparticles: Facile sol-gel synthesis for photocatalytic desulfurization of thiophene under visible light. *Journal of Alloys and Compounds*. 2020;823:153786.
 20. Hummers WS, Offeman RE. Preparation of Graphitic Oxide. *Journal of the American Chemical Society*. 1958;80(6):1339-1339.
 21. Kumar A, Singh AK, Tomar M, Gupta V, Kumar P, Singh K. Electromagnetic interference shielding performance of lightweight $\text{NiFe}_2\text{O}_4/\text{rGO}$ nanocomposite in X- band frequency range. *Ceram Int*. 2020;46(10):15473-15481.
 22. Mousavi-Kamazani M. Facile hydrothermal synthesis of egg-like BiVO_4 nanostructures for photocatalytic desulfurization of thiophene under visible light irradiation. *Journal of Materials Science: Materials in Electronics*. 2019;30(19):17735-17740.
 23. Mousavi-Kamazani M, Zarghami Z, Rahmatolahzadeh R, Ramezani M. Solvent-free synthesis of $\text{Cu}-\text{Cu}_2\text{O}$ nanocomposites via green thermal decomposition route using novel precursor and investigation of its photocatalytic activity. *Adv Powder Technol*. 2017;28(9):2078-2086.
 24. Investigation of structural and optical characteristics of CuO nanoparticles calcinated at various temperatures. *Indian J Chem Technol*. 2022.
 25. Zonarsaghar A, Mousavi-Kamazani M, Zinatloo-Ajabshir S. Sonochemical synthesis of CeVO_4 nanoparticles for electrochemical hydrogen storage. *International Journal of Hydrogen Energy*. 2022;47(8):5403-5417.
 26. Anju, Yadav RS, Pötschke P, Pionteck J, Krause B, Kuřitka I, et al. $\text{Cu}_x\text{Co}_{1-x}\text{Fe}_2\text{O}_4$ ($x = 0.33, 0.67, 1$) Spinel Ferrite Nanoparticles Based Thermoplastic Polyurethane Nanocomposites with Reduced Graphene Oxide for Highly Efficient Electromagnetic Interference Shielding. *Int J Mol Sci*. 2022;23(5):2610.
 27. Hu L, Li M, Cheng L, Jiang B, Ai J. Solvothermal synthesis of octahedral and magnetic CoFe_2O_4 -reduced graphene oxide hybrids and their photo-Fenton-like behavior under visible-light irradiation. *RSC Advances*. 2021;11(36):22250-22263.
 28. Nosheen E, Shah SM, Batool A, Ullah N, Hussain H, Ali I. Amphiphilic Z907 dye grafted ZnS/rGO and $\text{Zn}_{1-x}\text{Cd}_x\text{S}/\text{rGO}$ decorated nano-hybrid structures: Synthesis, characterization and applications in solid state dye sensitized solar cells. *Optik*. 2021;244:167609.